Line shapes and intensities of self-broadened O_2 $b\,^1\Sigma_g^+(v=1) \leftarrow X\,^3\Sigma_g^-(v=0)$ band transitions measured by cavity ring-down spectroscopy

D. Lisak,[1] P. Masłowski,[1] A. Cygan,[1] K. Bielska,[1] S. Wójtewicz,[1] M. Piwiński,[1]
J. T. Hodges,[2] R. S. Trawiński,[1] and R. Ciuryło[1]

[1]*Instytut Fizyki, Uniwersytet Mikołaja Kopernika, ul. Grudziadzka 5/7, 87-100 Toruń, Poland*

[2]*National Institute of Standards and Technology, 100 Bureau Drive, Gaithersburg, Maryland 20899, USA*

(Received 28 October 2009; published 12 April 2010)

We present high-resolution line-shape and line-intensity measurements of self-broadened O_2 $b\,^1\Sigma_g^+(v=1) \leftarrow X\,^3\Sigma_g^-(v=0)$ band (B-band) transitions measured using the frequency-stabilized cavity ring-down spectroscopy technique under relatively low pressure conditions. We give line-shape parameters describing collisional broadening and shifting, and we treat line narrowing in terms of Dicke narrowing or the speed dependence of collisional broadening. We indicate the importance of the line-narrowing effect which, if neglected, changes the experimentally determined collisional broadening coefficients by up to 48%. We report measured line intensities with relative uncertainties below 0.7% and compare these measurements to published data.

DOI: 10.1103/PhysRevA.81.042504 PACS number(s): 33.70.−w

I. INTRODUCTION

The oxygen molecule, O_2, has two low-lying excited electronic states, $a\,^1\Delta_g$ and $b\,^1\Sigma_g^+$, which are approximately 7888 cm^{-1} and 13,122 cm^{-1}, respectively, above the $X\,^3\Sigma_g^-$ ground state. Magnetic dipole transitions between these electronic states, $a \leftarrow X$, $b \leftarrow X$, and $b \leftarrow a$, give rise to a number of rovibronic bands in the visible and near-infrared spectral regions, which feature prominently in the absorption of solar radiation by the Earth's atmosphere. Because the mixing ratio of O_2 in the atmosphere is uniform and relatively constant over long path lengths, these bands can also be used in a number of land- and satellite-based remote-sensing applications such as the determination of cloud-top heights [1], surface pressure [2,3], column temperature [4], and CO_2 concentration [5–8]. These measurement techniques require high-accuracy spectroscopic line parameter data (e.g., intensities, widths, and positions), which are based on the judicious combination of laboratory measurements and theoretical models.

Here we focus our attention on the O_2 $b\,^1\Sigma_g^+(v=1) \leftarrow X\,^3\Sigma_g^-(v=0)$ band (referred to hereinafter as the B band), which occurs near the wavelength $\lambda = 687$ nm. Properties of the O_2 B band were first reported by Babcock and Herzberg [9] in their observations of solar spectra, and subsequently, Giver *et al.* [10] measured this band in the laboratory using a long-pass White cell and grating spectrometry. O'Keefe [11] and Scherer *et al.* [12] probed the O_2 B band with a pulsed laser in what was the first demonstration of cavity ring-down spectroscopy (CRDS) for measuring the absorption spectrum of a gas. Additional CRDS measurements of this band include those of Xu *et al.* [13] and those of Motto-Ros *et al.* [14], the latter study being based on a continuous-wave CRDS laser technique. Motto-Ros *et al.* achieved signal-to-noise ratios (SNRs) up to 1000:1, which allowed them to observe collisional narrowing effects. Cheah *et al.* [15] measured line intensities, collisional widths, and shifts of many transitions of the O_2 B band using a Fourier-transform spectrometer. Also, Barnes and Hays [16] measured pressure broadening and shifting in the O_2 B band using photoacoustic spectroscopy. Their data were used to correct atmospheric wind measurements made from a satellite-borne Doppler imager [16]. A recent application of O_2 B-band spectroscopy includes satellite-based solar occultation absorption measurements used to determine temperature and pressure profiles in the Earth's atmosphere [4].

In the remainder of the article, we discuss the importance of line-shape effects for the accurate determination of line intensities and line-shape parameters, and we present a line-shape study of several self-broadened transitions of the O_2 B band. We use frequency-stabilized (FS)-CRDS [17,18] to measure spectra over the pressure range 0.13–3.3 kPa. At these conditions, the line shapes are dominated by Doppler broadening. The FS-CRDS technique has been proven to yield high-quality spectra practically free from instrumental distortion [19–21]. For the transitions and pressure range investigated in this study, the incorporation of line-narrowing effects introduces an important and nonnegligible correction to the Voigt profile. We found that the fitted collisional broadening coefficients determined from the Voigt profile were up to 48% smaller than those derived using profiles that account for speed-dependent effects (speed-dependent Voigt profile, SDVP) or Dicke narrowing (Galatry profile, GP). Such a large correction to the collisional broadening coefficient can be important for many applications based on high-precision, quantitative spectroscopy of O_2. We also report measured absolute line intensities and compare these results to values from the literature.

II. LINE-SHAPE EFFECTS

The analysis of line shapes measured in gas-phase absorption spectra provides important data for validating theoretical models of atomic and molecular interactions and dynamics. The ability to accurately model line shape can also be important in a variety of spectroscopic applications such as trace gas detection, atmospheric composition analysis, remote pressure and temperature measurement, and human breath analysis for medical purposes (see, e.g., Chap. VII of [22]). However, it is well known that the theoretical Voigt profile (VP), which takes

into account Doppler broadening and collisional (pressure) broadening and shifting of spectral lines, is generally not valid because of its assumption of statistical independence of collisional and Doppler broadening [23]. Nevertheless, most spectroscopic databases (including HITRAN [24], which is the most comprehensive and commonly used database in the atmospheric spectroscopy community) provide line-specific data suitable for calculating only the Voigt profile, and in most applications, both the speed-dependent effects and collisional narrowing are neglected because their influence on line shapes is considered to be small.

Berman [25] derived the SDVP by incorporating into the line-shape model the dependence of collisional effects on the absorber or emitter speed. Moreover, assumptions made in deriving the Doppler component of the line profile are also not valid for physical conditions where gas pressure is not infinitely small. Specifically, the mean free path of the absorber (or emitter) decreases with increasing gas pressure, leading to an effective decrease of average absorber displacement (in a given time) along the direction propagation of the light beam. If this reduction of the mean free path length is not negligible compared to the wavelength of absorbing light, it may lead to collisional narrowing of the line (Dicke narrowing) [26]. Here we note that a simple comparison of the mean free path and transition wavelength does not enable one to predict the magnitude of Dicke narrowing for a given transition. Generally, quantum-mechanical calculations are required (see, e.g., [27,28]). In the framework of semiclassical line-shape theory, the reduction of collisional narrowing can be attributed to correlations between phase- and velocity-changing collisions [29,30]. The collisional narrowing effect was observed in many studies and most often analyzed using two semiclassical models of molecular collisions, leading to the GP [31] and the Nelkin-Ghatak profile (NGP) [29,32], based on soft- and hard-collision models, respectively. We note that the Nelkin-Ghatak line shape is also called the Rautian profile. More complicated models, which consider both soft and hard collisions, correlations between velocity- and phase-changing collisions which effectively reduce the Dicke narrowing effect, and the speed-dependent effects [33–35], as well as models using more realistic description of collisions [36–39], have been derived and used for data analysis (see [22]).

It is often difficult to determine solely from the quality of fits to experimental profiles the relative contributions to the line shape of speed-dependent collisional broadening and Dicke narrowing. This ambiguity occurs because both mechanisms can tend to reduce the line width. Ritter and Wilkerson [40] first identified this problem, which was subsequently investigated by others [23,41–43]. To ensure that fitted line-shape parameters are constant or vary linearly with pressure, three conditions usually need to be met. First, the measured spectra must have sufficient SNR to resolve relatively small changes in the line shape. Second, measurements must be acquired over a wide pressure range, and third, the set of spectra corresponding to various pressures need to be simultaneously fit to eliminate pressure-dependent correlations between fitted parameters [21,44–46]. However, even when all three conditions are met but the physical effects mentioned earlier are ignored, it is sometimes impossible to determine line intensities and line-shape parameters with subpercent level of uncertainties that are required in many modern applications.

III. EXPERIMENTAL SETUP

The experimental spectra were measured using a FS-CRDS spectrometer located at the Institute of Physics of Nicolaus Copernicus University in Toruń, Poland. The FS-CRDS system is essentially identical to those developed at the National Institute of Standards and Technology (NIST) in Gaithersburg, Maryland [17–19]. The ring-down cell, which was constructed at NIST, comprises an optical resonator formed by two concave mirrors, having 1 m radius of curvature, in a nonconfocal configuration. The nominal cavity length is about 73 cm. The mirrors have a high reflectivity, $R = 0.99973$, at the wavelength $\lambda = 687$ nm of our spectral measurement, and $R = 0.98$ at $\lambda = 633$ nm, corresponding to the wavelength of the reference HeNe laser used to actively stabilize the cavity length. The longtime frequency stability of the HeNe laser is below 2 MHz per 8 hours. To generate the error signal required for active control of the cavity length, the HeNe frequency is modulated around the transmission peak of the ring-down cavity transverse electromagnetic mode TEM_{00} with an acousto-optical modulator (AOM). The HeNe laser frequency has a modulation depth of ± 6.5 MHz with modulation frequency 100 kHz. The low-bandwidth feedback signal controls displacement of one of the cavity mirrors mounted on the piezoelectric actuator to maintain a constant optical path length between mirrors. A low-pass filter at 100 Hz was applied to reduce noise which can be introduced by the feedback loop. Therefore only slow thermal drift of the cavity is compensated by this feedback loop.

The probe laser (external cavity diode laser) is mode matched to the TEM_{00} mode of the ring-down cavity, and its frequency is slowly modulated around the local cavity resonance. The transmission signal of the probe laser beam through the cavity triggers a second AOM (working at 200 MHz) to rapidly turn off the laser beam on a timescale shorter than 50 ns. This event triggers acquisition of the ring-down signal, which is measured by a 10-MHz-bandwidth Si-PIN detector. For data acquisition, we use a 14-bit, analog-to-digital converter working at a sampling rate of 25 MHz. Typical ring-down time constants are about 9 μs for an empty cavity. At each frequency step of the spectrum, 300 ring-down decays are recorded and their time constants are averaged. In order to change the probe laser frequency, it is tuned to the next TEM_{00} mode of the cavity and relocked to it. This mode-by-mode tuning procedure provides a spectrum frequency axis with high resolution and having a point spacing equal to the cavity-free spectral range (FSR). The value of FSR was 203.434(4) MHz, measured with a wavemeter having a combined uncertainty of 60 MHz, using the technique described in Ref. [17]. The precision of the frequency axis is limited only by the stability of the reference HeNe laser. Also, the spectral point density can be increased by tuning the RF frequency on the AOM, which shifts the optical frequency of the HeNe laser. The AOM tuning range is 250–400 MHz and is doubled using a double-pass configuration [17]. In this fashion, the comb of cavity modes locked to the HeNe laser tracks the frequency change of the AOM. At the same time, the probe laser is

locked to one of the cavity modes. The empty cavity and probe laser beam were aligned to yield flat baseline cavity losses without any measurable interference fringes. This FS-CRDS configuration yields SNRs of O_2 spectra exceeding 2000:1 with an exceptionally linear frequency axis and insensitivity to probe laser power fluctuations. The applicability of FS-CRDS for high-precision measurements of spectral line shapes and intensities was verified in previous near-infrared studies of H_2O [19–21] and O_2 [47–49] spectra.

For sample preparation, we used high-purity oxygen (99.995% of $^{16}O_2$ at natural isotopic abundance having a $^{16}O_2$ molar fraction of 0.995262). This sample gas was delivered to the stainless steel ring-down cell through a vacuum system made of electropolished stainless steel. The gas pressure was measured with a calibrated, temperature-stabilized capacitance manometer having a relative uncertainty of 0.05%, and the cavity temperature was measured by a Hg thermometer with a standard uncertainty of 0.1 K.

IV. RESULTS AND DISCUSSION

In this study, we chose six R-branch transitions of the O_2 B band, and their wave numbers, $\tilde{\nu}_0$, line intensities, S, and quantum assignments are given in Table I. These data were taken from the HITRAN 2008 database [24]. For the first (strongest) transition, the self-broadened line profiles were measured at pressures p between 0.13 and 1.2 kPa. All other transitions were measured together on a common frequency axis, the pressure range being varied from 1.1 to 3.3 kPa. Henceforth the measured transitions will be referred to by the numeric identifiers given in the first column of Table I.

A. Line-shape analysis

We fit VPs to the experimental spectra as well as line profiles, taking into account collisional (Dicke) narrowing (GP [31] and NGP [29,32]). We also used profiles that model the speed dependence of the collisional width (SDVP [25]). Finally, we used the speed-dependent Nelkin-Ghatak profile (SDNGP), which includes both Dicke narrowing and speed-dependent effects [29,50]. In the cases of the SDVP and SDNGP, we used a quadratic model for the speed dependence of collisional broadening as given by Priem *et al.* [41]. To this end, the reduced speed-dependent collisional width function

TABLE I. List of measured O_2 B-band transitions with transition wave numbers $\tilde{\nu}_0$, intensities S at temperature 296 K, and lower state energies E''. Quantum assignments are in terms of the rotational angular momentum N and total angular momentum J, where the double prime indicates the lower state. Data are taken from HITRAN [24].

Line no.	$\tilde{\nu}_0$ (cm^{-1})	S [cm^{-1}/(molecule/cm^2)]	E″ (cm^{-1})	Assignment ΔN N'' ΔJ J''
1	14546.008735	5.886×10^{-25}	79.5646	R7 Q8
2	14556.572680	2.962×10^{-26}	931.3374	R25 Q26
3	14557.231507	2.262×10^{-25}	438.4414	R17 Q18
4	14557.552300	5.412×10^{-26}	791.0332	R23 Q24
5	14557.878331	1.498×10^{-25}	544.5651	R19 Q20
6	14557.986348	9.294×10^{-26}	662.1021	R21 Q22

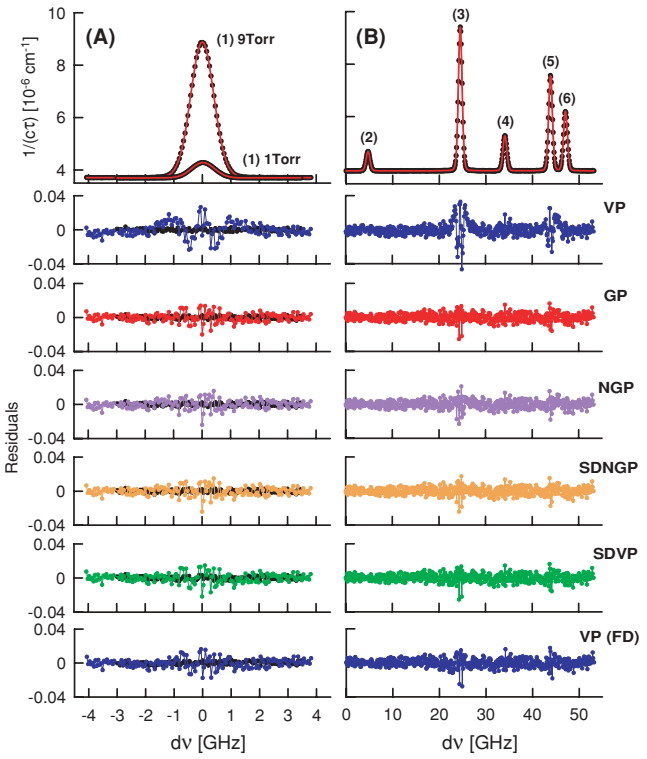

FIG. 1. (Color online) The experimental spectra of self-broadened oxygen lines and residuals from fits of different models [VP, GP, NGP, SDNGP, SDVP and VP(FD)] to experimental profiles at pressures (A) 1 and 9 Torr for line 1 and (B) 25 Torr for lines 2–6.

$B_W(x)$ [51,52] was approximated by the following function:

$$B_W(x) = 1 + a_W(x^2 - 3/2). \quad (1)$$

Here x denotes the reduced absorber velocity and a_W is a fitted parameter. We ignored the speed dependence of collisional shifting because of the small values of self-shifting for the transitions investigated here. To evaluate the line-shape profiles, we used the formulas from Ref. [52].

We present measured spectra of the self-broadened O_2 lines in Fig. 1. Below are residuals R from fits of different models to the experimental profiles for the highest pressures measured: 1.2 kPa (9 Torr) for line 1 and 3.3 kPa (25 Torr) for lines 2–6. In the case of the VP, which is based on a fixed Doppler width, γ_D, corresponding to the gas temperature, inspection of the fit residuals clearly indicates that this profile cannot properly model the measured spectra, and consequently, line-narrowing effects must be taken into account. On the other hand, the residuals corresponding to all other profiles considered here are equally good. This result agrees with observations of other authors for different molecular systems (see, e.g., [21,40,41,43]). For low pressures, they found that the observed line narrowing could be described equally well using models that include either Dicke narrowing or the speed-dependent effects. The VP(FD) in Fig. 1 denotes the Voigt profile with fitted Doppler width.

In Fig. 2 we present the full width at half maximum (FWHM) collisional width, γ_L, of the self-broadened O_2 lines 1 and 3 as a function of O_2 concentration N. The

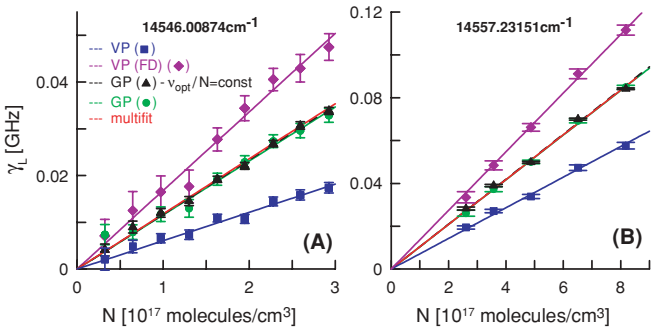

FIG. 2. (Color online) Dependence of the collisional width (FWHM), γ_L, of the self-broadened O_2 lines on O_2 concentration N for (A) line 1 and (B) line 3. See text for details.

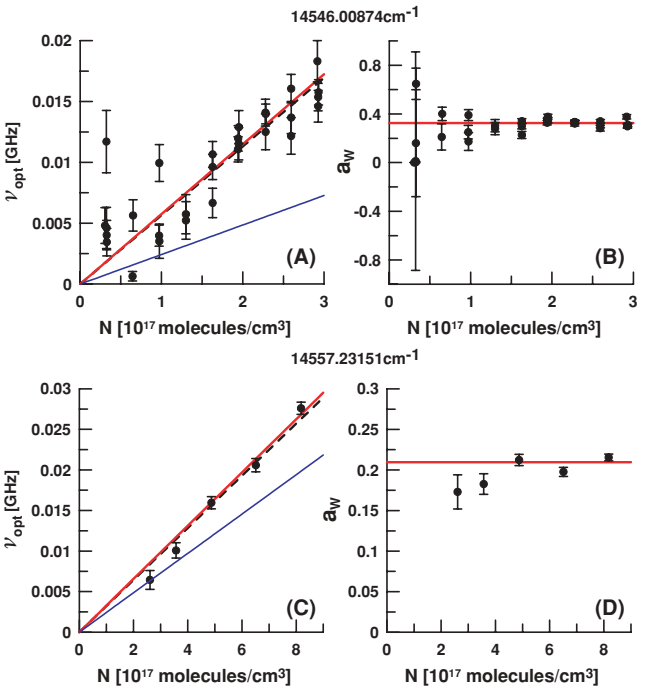

FIG. 3. (Color online) (A, C) Collisional narrowing parameter, ν_{opt}, obtained from the fits of GP and (B, D) the parameter of the quadratic speed dependence of collisional broadening, a_W, obtained from fits of the SDVP to the experimental spectra of transitions (A, B) 1 and (C, D) 3. See text for details.

circular (green) points are the γ_L values obtained from individual fits of the GP to spectra for each pressure. The red straight line corresponds to the collisional width obtained from multispectrum fits of the GP to the measured spectra. In the multispectrum fitting procedure, a set of spectra corresponding to multiple pressures are fit simultaneously, and the values of collisional width, γ_L, and frequency of optical collisions, ν_{opt}, are constrained to vary linearly with gas concentration. Using these constraints, the linear coefficients, $\Gamma = \gamma_L/N$, and $\beta = \nu_{\text{opt}}/N$, are the fitted parameters. This multispectrum fitting procedure mitigates the problem of correlations between fitted parameters. At low pressures, as investigated here, small changes in the total modeled line width can be realized by changing either the broadening width, γ_L, or the narrowing parameter, ν_{opt}. Furthermore, with regard to the quality of the fits, these two cases are indistinguishable over some parameter range that is dependent on the SNR of the measured profiles. This effect is clearly seen in Fig. 2 for the individually fitted γ_L at the lowest pressures of both O_2 lines 1 and 3, for which the fitted γ_L deviates from a linear dependence on concentration N. The black triangular symbols in Fig. 2 denote the γ_L values that were also individually fitted with the GP for each concentration, but in this case, the collisional narrowing parameters ν_{opt} were constrained to those values obtained from the multispectrum fit. Clearly the linearity of the γ_L versus N correlation is improved in comparison to the results in which γ_L and ν_{opt} were individually fitted. The values of the collisional widths, γ_L, obtained from SDVP fits to the measured profiles are similar to those shown in Fig. 2 for GP fits.

The blue square points in Fig. 2 correspond to the γ_L values resulting from fits of the VP to the experimental data. We note that all our fits were done with the Doppler width of the lines constrained to the value corresponding to the gas temperature. It is interesting that the relative difference between the γ_L values obtained from the VP and GP fits is 48% and 27% for lines 1 and 3, respectively. Such a large difference obviously cannot be treated as a small effect and indicates the importance of line-narrowing effects on the overall line shape. This result has potential applications when the Doppler width greatly exceeds the collisional width. For comparison, we also present in Fig. 2 γ_L values obtained from the VP with fitted Doppler width VP(FD). These fits, in contrast to the fits of VP with constrained Doppler width, give γ_L values that are systematically bigger than GP fits. With the same number of fitted parameters, uncertainties of the γ_L from VP(FD) fits are significantly greater than those from GP fits.

In Fig. 3 we plot the values of the collisional narrowing parameter, ν_{opt}, obtained from fits of the GP and a parameter of the quadratic speed dependence of collisional broadening, a_W [see Eq. (1)], obtained from fits of the SDVP to the experimental spectra of transitions 1 and 3. The symbols with error bars indicate values achieved from the individual fits for each concentration, and the red straight lines correspond to the coefficients obtained from the multispectrum fit. As mentioned before, the correlation between parameters responsible for broadening, γ_L, and for narrowing (ν_{opt} for the GP or a_W for SDVP) of the line is more evident for smaller concentrations, N. This effect increases the uncertainty, shown as error bars, in ν_{opt} and a_W as N decreases. Moreover, in Fig. 3(a), there is a clear correlation between deviations in ν_{opt} and γ_L, both of which are underestimated at the lowest concentrations. However, when taken together, they give the correct total line width of these transitions. This result is further evidence that the line-shape parameters obtained from the multispectrum fit procedure are more reliable than those derived from individual fits at each gas concentration.

Simplified treatment of Dicke narrowing and velocity-changing collisions neglecting correlation with the collisional broadening and shifting of the line allows us to estimate the frequency of velocity-changing collisions [22,29,53]. In such a case, the frequency of velocity-changing collisions $\nu_{\text{diff}} = k_B T/(2\pi m_A D)$ is related to the mass diffusion coefficient D [26,29,31] and proportional to the gas pressure or

concentration. In this expression, k_B is Boltzman constant, m_A is the absorber mass, and T is gas temperature. The mass diffusion coefficient can be estimated in the framework of the first-order approximation [54,55], which is widely used. We carried out this calculation assuming the Lennard-Jones potential for description of O_2-O_2 interaction. The Lennard-Jones potential was used with parameters $\sigma = 3.433 \times 10^{-10}$ m and $\varepsilon/k_B = 113$ K listed by Hirschfelder *et al.* [54]. For the atmospheric pressure and the averaged gas temperature $T = 297.01$ K, the gas concentration is $N = 247.09 \times 10^{17}$ molecules/cm^3, and the evaluated $D = 0.205$ cm^2/s corresponds to $\nu_{\text{diff}} = 0.6$ GHz. To verify how important in this calculation is choice of the interaction model, we also used the anisotropic potential given by Mingelgrin and Gordon [56], which was averaged over all possible orientations in the way described in Ref. [57]. It was found that the mass diffusion coefficient calculated for the potential of Ref. [56] is smaller about 5% then the value obtained for Lennard-Jones potential even if both potentials are significantly different.

The frequency of velocity-changing collisions, ν_{diff}, linearly dependent on the gas concentration evaluated from the mass diffusion coefficient, D, has been marked on Fig. 3 as a blue solid line. As can be seen from this plot, observed ν_{opt} for these two lines is significantly bigger than the calculated value ν_{diff}. It very strongly indicates that the speed dependence of the collisional broadening is present in the investigated case. Here one can find some analogy to results obtained by May and his coworkers [23,58,59]. Authors demonstrated that for some perturbers, observed narrowing cannot be explained only by velocity-changing collisions but also the speed-dependent effects ought to be taken into account in the analysis of measured spectra.

In Fig. 4(a), we compare the collisional self-broadening coefficients, $\Gamma = \gamma_L/N$, of six O_2 lines obtained from fits of the different line-shape profiles, VP, GP, and SDVP, to the experimental data. They are plotted as a function of the upper state total angular momentum quantum number J'. We find the usually observed decrease in Γ with increasing rotational energy when either the GP or SDVP are fitted, except for one point having the highest uncertainty. It is interesting that we observe the opposite dependence, namely, increasing Γ with increasing J', when the VP is fit to our measured spectra. In Fig. 4(b), we present the fitted collisional narrowing coefficients, $\beta = \nu_{\text{opt}}/N$, from the GP fits and the speed-dependence parameter, a_W, from the SDVP fits as a function of J'. The blue solid line marks the value of the coefficient $\beta_{\text{diff}} = \nu_{\text{diff}}/N = 0.243 \times 10^{-19}$ GHz/(molecule/cm^3). For both fitted profiles, the line-narrowing effect decreases with increasing angular momentum J'. This dependence is consistent with the observed difference between the Γ coefficients for the VP and GP or SDVP presented in Fig. 4(a): When the line-narrowing effect is not taken into account (in the VP), the collisional broadening Γ is underestimated.

As was mentioned earlier, the pressure range investigated here is so low that the SDVP and GP describe the experimental spectra equally well at our signal-to-noise level. Similar observations were made by Ritter and Wilkerson [40] for pressure-broadened A-band lines of O_2. For the combined, approximated speed-dependent Galatry profile (aSDGP) [60] with quadratic speed-dependent broadening, Priem *et al.* [41]

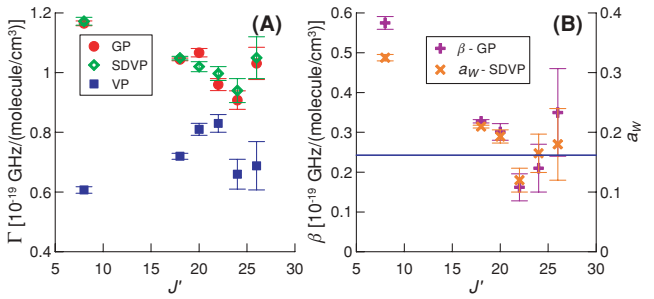

FIG. 4. (Color online) (A) Comparison of the collisional self-broadening coefficients, Γ, of six oxygen lines obtained from fits of different line shape profiles, VP, GP, and SDVP, to experimental data plotted as a function of J'. (B) Collisional narrowing coefficients β from GP fits and the speed-dependence parameter, a_W, from the SDVP fits as a function of J'.

showed that the effective narrowing of this profile, compared to the VP, is dominated by a term proportional to $\nu_{\text{opt}} + 3a_W\gamma_L/2$ in the low-pressure regime. This leads to a very strong correlation between fitted parameters ν_{opt} and a_W, even if the multispectrum fit procedure is used. Therefore we cannot independently determine both Dicke narrowing and speed-dependent contributions for either the aSDGP or the SDNGP. For each transition, we find that ν_{opt} obtained from the GP fit equals, to within the experimental uncertainty, the value of $3a_W\gamma_L/2$ determined from the SDVP fit. This result was previously reported for CO lines [41].

B. Collisional shifting

The FS-CRDS technique allows us to place experimental spectra measured at different gas pressures on a common frequency axis if the cavity remains locked to the reference HeNe laser during the change of gas pressure. This technique was first introduced by Robichaud *et al.* [61] and subsequently applied to the measurement of pressure shifting by air- and self-broadened O_2 $b\,^1\Sigma_g^+(v=0) \leftarrow X\,^3\Sigma_g^-(v=0)$ band (A-band) transitions [47]. Its implementation requires that one precisely account for dispersion, $dn/d\lambda$, in the refractive index n of the ring-down cavity sample gas. Changes in the gas pressure alter n at the HeNe laser reference wavelength, and in response, the active cavity stabilization servo adjusts the cavity length so that the optical path length (product of geometric length and refractive index at the reference laser wavelength) does not change. However, in the vicinity of the probe laser wavelength, the cavity resonances shift slightly because of dispersion in the index of refraction of the cavity medium. This systematic effect can be precisely calculated in terms of the known wavelengths, pressure, temperature, and composition of the sample gas [61]. Here we use the accurate formulas for the refractive index of O_2 given by Zhang *et al.* [62].

For a given HeNe laser frequency, we have the following equation for the frequency ν_j of the longitudinal mode of order j of the cavity:

$$\nu_j = \frac{c}{2n_j(p_1,T_1)l_1}j, \tag{2}$$

where c is the speed of light, $n_j(p_1,T_1)$ is the refractive index of O_2 at the frequency ν_j, pressure is p_1 and temperature

is T_1, and l_1 is the cavity length. Here we have neglected the ring-down mirror phase-shift terms which have a small contribution to the correction of our frequency axis. If the pressure is changed with the cavity continuously locked to the HeNe frequency, then we can write a second equation for the pressure p_2 and temperature T_2:

$$\nu_j = \frac{c}{2n_j(p_2,T_2)l_2}j, \tag{3}$$

where l_2 is the cavity length at p_2 and T_2. The cavity servo changes l_1 to l_2 to keep the TEM_{j00} resonance at frequency ν_j. Comparing the preceding two equations, the new cavity length is

$$l_2 = \frac{n_j(p_1,T_1)}{n_j(p_2,T_2)}l_1. \tag{4}$$

For the probe laser frequency, ν_q, the corresponding equations for (p_1,T_1) and (p_2,T_2) are

$$\nu_q(p_1,T_1) = \frac{c}{2n_q(p_1,T_1)l_1}q, \tag{5}$$

$$\nu_q(p_2,T_2) = \frac{c}{2n_q(p_2,T_2)l_2}q, \tag{6}$$

where q is the mode order of the cavity at the probe laser frequency. We note that the probe laser is locked to the cavity, so the correction to the frequency axis of the probe laser $\Delta\nu_q$ is

$$\begin{aligned}\Delta\nu_q &= \nu_q(p_2,T_2) - \nu_q(p_1,T_1)\\ &= \nu_q(p_1,T_1)\left[\frac{n_j(p_2,T_2)n_q(p_1,T_1)}{n_q(p_2,T_2)n_j(p_1,T_1)} - 1\right],\end{aligned} \tag{7}$$

which is equivalent to the result given by Robichaud *et al.* [61] provided $n - 1 \ll 1$.

Our measured collisional self-shifting coefficients Δ turned out to be an order of magnitude smaller than the self-broadening coefficients and were comparable to their combined standard uncertainties. Clearly a wider pressure range would be required to improve these results. In Fig. 5 we present measured shifts of lines 1 and 3 versus O_2 concentration, and the error bars indicate the combined standard uncertainties. The small values of the collisional shift agree with our observations of symmetrical line shapes for all lines that we investigated because one potential source of line asymmetry is the speed dependence of collisional shifting. To our knowledge, there are no data available in the literature on self-shifting of these O_2 transitions.

C. Measurement of line intensities

CRDS provides a direct measure of the light losses from the time constant of the ring-down decay τ:

$$\frac{1}{c\tau(\nu)} = \alpha_{bg}(\nu) + \alpha(\nu), \tag{8}$$

where $\alpha(\nu)$ is the absorption coefficient of the sample gas. The term α_{bg} is the spectrum background and corresponds to the mirror losses and all light losses in the cavity, excluding absorption by the gas sample. For a single, isolated transition,

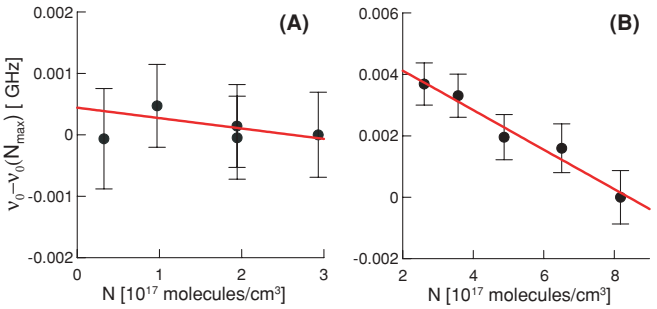

FIG. 5. (Color online) Experimental collisional shifting of (A) line 1 and (B) line 3 vs. O_2 concentration. Error bars indicate combined standard uncertainties.

$\alpha(\nu)$ is related to the line intensity, S, gas concentration, N, and normalized line-shape function, $g(\nu-\nu_0)$, by

$$\alpha(\nu) = cNSg(\nu-\nu_0). \tag{9}$$

After integrating over the frequency, ν, one obtains the line area $A = \int \alpha(\nu)d\nu$. The line intensity for a given gas temperature, T, can be calculated from the relation

$$S(T) = \frac{A}{cN}. \tag{10}$$

In Fig. 6 the line areas, A, of all the O_2 lines investigated here are plotted versus gas concentration, N. In all cases, we observed no deviation from the expected linear dependence of A with N. The results presented here are based on GP fits to the experimental data, although we should note that line areas from the SDVP, NGP, SDNGP, and even VP are identical to within their standard uncertainties. The relative standard uncertainties, $u(S)/S$, of the line intensities, S, determined from the slopes of the linear functions, $A(N)$, presented in Fig. 6 are below 0.7%. This value also accounts

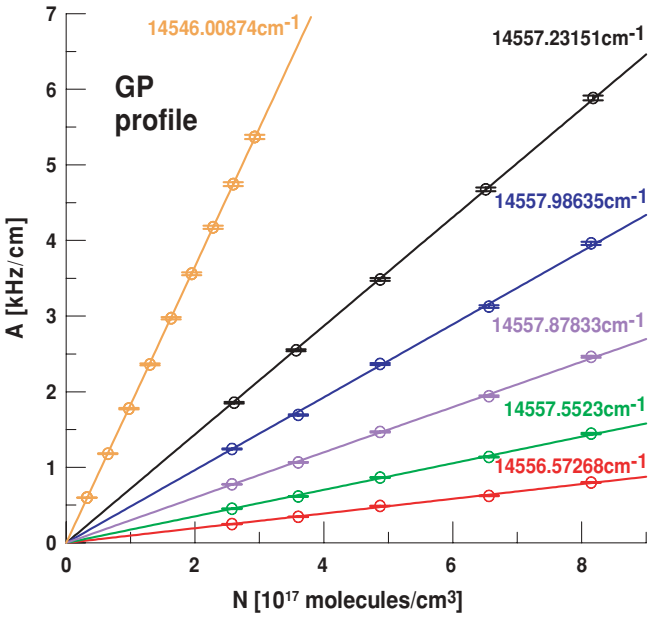

FIG. 6. (Color online) Line areas, A, of the O_2 lines investigated here, determined from GP fits and plotted as a function of gas concentration N.

TABLE II. Experimental line-shape coefficients and intensities of self-broadened O_2 lines obtained from fits of different line-shape models: GP, SDVP, and VP to experimental data, and their combined standard uncertainties. Line number corresponds to the line number from Table I. Line intensity S is in units 10^{-25} cm^{-1}/(molecule/cm^2), Γ is collisional broadening, β is collisional narrowing, Δ is collisional shifting in units 10^{-19} GHz/(molecule/cm^3), and speed-dependence parameter a_W is dimensionless.

	GP				SDVP			VP	
Line no.	S	Γ	β	Δ	S	Γ	a_W	S	Γ
1	6.113(32)	1.165(8)	0.575(16)	−0.017(13)	6.116(32)	1.172(13)	0.3251(53)	6.077(32)	0.607(11)
2	0.318(2)	1.031(54)	0.35(11)	−0.09(6)	0.317(2)	1.05(7)	0.18(6)	0.3147(21)	0.688(81)
3	2.371(13)	1.0446(42)	0.3281(42)	−0.0643(72)	2.381(13)	1.049(6)	0.2096(23)	2.355(13)	0.72(1)
4	0.5705(35)	0.908(31)	0.21(6)	−0.053(52)	0.5769(35)	0.94(4)	0.165(32)	0.5722(35)	0.66(5)
5	1.59(1)	1.067(14)	0.301(21)	−0.113(41)	1.59(1)	1.020(17)	0.193(11)	1.58(1)	0.81(2)
6	0.990(6)	0.96(2)	0.162(34)	−0.157(45)	0.990(6)	0.997(23)	0.12(2)	0.986(6)	0.83(3)

for uncertainties in pressure, temperature, and the frequency axis determination. Since we worked with nonisotopically enriched samples, the reported $^{16}O_2$ intensities are weighted to the natural terrestrial isotopic abundance, which is consistent with the convention used in HITRAN [24].

We summarize our experimental results in Table II, in which we compare our fitted line-shape parameters obtained using the three models VP, GP, and SDVP. As emphasized before, we found large relative differences between the collisional broadening coefficients obtained from the VP, GP, and SDVP fits (13%–48%). Line intensities reported in Table II are corrected to the standard reference temperature $T_r = 296$ K using the lower state energies given in Table I and partition function data from HITRAN [24]. In all cases, this correction was smaller than 1%.

D. Analysis of line-intensity variation with rotational quanta

From Gamache *et al.* [63], we find the theoretical dependence of S on the lower state total angular momentum quantum number J'' in terms of the band intensity, S_b, and band center wave number, $\tilde{\nu}_b$, as

$$S(J'') = \frac{C S_b g \tilde{\nu}(J'') \zeta(J'') e^{-E''(J'')hc/k_B T}}{Q(T)\tilde{\nu}_b}, \qquad (11)$$

where h is Planck's constant, C is a dimensionless normalization factor ensuring that $\sum S(J'') = S_b$, $Q(T)$ is the total partition function, g is a degeneracy factor equal to 3 for the $X\,^3\Sigma_g^-$ ground state, and $\zeta(J'')$ is the branch-dependent Hönl-London factor which describes the intrinsic strength of the transition independently of the Boltzmann factor, $Q^{-1}e^{-E''(J'')hc/k_B T}$. The Hönl-London factors for $b\,^1\Sigma_g^+ \leftarrow X\,^3\Sigma_g^-$ transitions depend on the coupling of the electron spin to the molecular axes in the $X\,^3\Sigma_g^-$ state. Ritter and Wilkerson [40] summarized expressions for $\zeta(J'')$ for $b\,^1\Sigma_g^+ \leftarrow X\,^3\Sigma_g^-$ transitions of O_2. Of these, the form of $\zeta(J'')$ given by Watson [64] is the most general. Watson specified the coupling of the electron spin to the internuclear axes for O_2 in terms of the effective Hamiltonian of the triplet ground state. In this case, the effective coupling is intermediate between Hund's type a (electron spin coupled to the internuclear axis) and Hund's type b (electron spin coupled to the molecular rotation axis) [65]. For the effective Hamiltonian of the $X\,^3\Sigma_g^-$ state, Watson gives the precise coupling in terms of the rotational energy spacing ($B = 1.438$ cm^{-1}), the spin-rotation ($\gamma = -8.43 \times 10^{-3}$) coupling constant, and the spin-spin ($\lambda = 1.985$ cm^{-1}) coupling constant. The Watson expressions for $\zeta(J'')$ are branch-dependent and for the RQ-branch lines presented here have the form $\zeta(J'') = S^2_{J''}(2J''+1)/2$, where $S^2_{J''}$ also depend on B, and the coupling constants γ and λ [40].

We present in Fig. 7 our set of six measured (GP fits) line intensities (triangles) and all lines of the O_2 B band that are reported in HITRAN (circles). To compare lines from the R and P branches, we have defined the angular momentum parameter $m = J'' + 1$ for R-branch lines ($\Delta N = 1$) and $-J''$ for P-branch lines ($\Delta N = -1$). Our measured intensities are in good qualitative agreement (but systematically high) with the corresponding HITRAN values and show similar dependence on m. The calculated intensities from Eq. (11) (using the Watson expressions for $\zeta(J'')$ and $S_b = 1.49 \times 10^{-23}$ cm/molecule [63]) are in good agreement with HITRAN (less than 1% difference) for $m > 0$ (R branch) but systematically become smaller than the HITRAN intensities for $m < 0$ (P branch), the maximum difference being about 4% at $m = -42$. We were unable to find a consistent

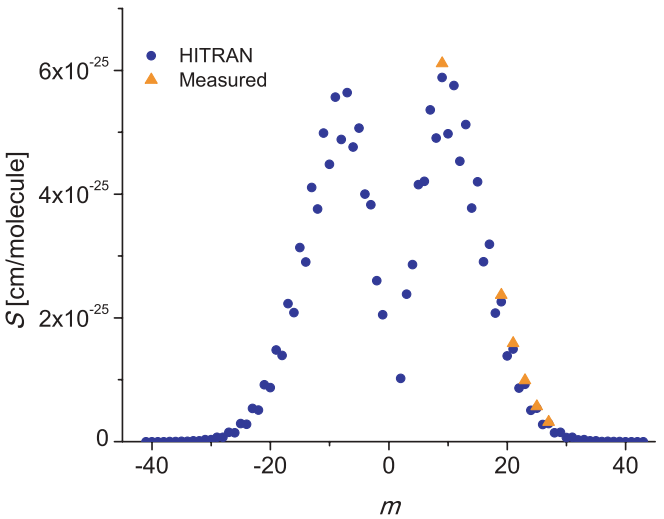

FIG. 7. (Color online) Our measured O_2 B-band line intensities (triangles), S, and HITRAN values (circles) vs. rotational quantum number, m.

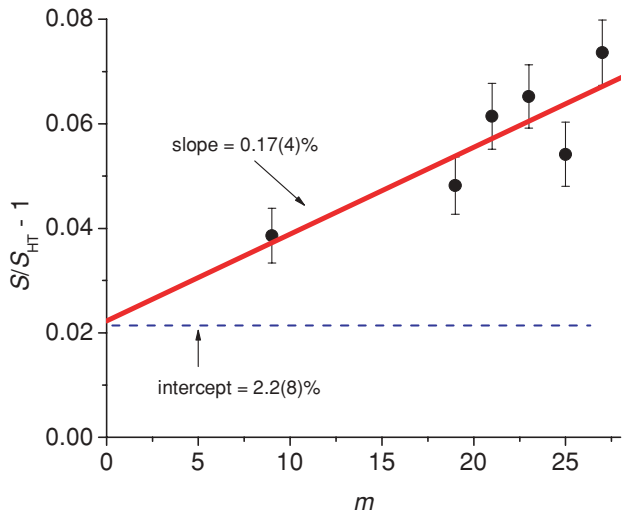

FIG. 8. (Color online) Fractional difference between our line intensities, S, and HITRAN values, S_{HT}. The solid line is a linear regression, and the error bars correspond to combined relative standard uncertainties of our measured intensities.

description in the literature of the functional form of $\zeta(J'')$ which was used to generate the HITRAN line list. However, the HITRAN line intensities for the O_2 B band $b\,^1\Sigma_g^+(v=1) \leftarrow X\,^3\Sigma_g^-(v=0)$ and O_2 A band $b\,^1\Sigma_g^+(v=0) \leftarrow X\,^3\Sigma_g^-(v=0)$ have an identical dependence on J'' and branch assignments that are consistent with Eq. (11). This comparison indicates that the same $\zeta(J'')$ factors were used in HITRAN to generate the intensities for both bands.

As can be seen in Fig. 8, our measured intensities are systematically higher than the corresponding reported HITRAN values, with the fractional difference increasing from 3% to 7.5% as $m = J'' + 1$ increases from 9 to 27. A linear regression to the data yields a slope and y intercept of 0.17(4)% per m and 2.2(8)% per m, respectively. Assuming a similar trend were to persist over the entire band (which spans positive and negative m values) implies that the HITRAN band intensity would be approximately 2% smaller than our band-integrated measurements.

Because we expect the rotational dependence of line intensities to be similar for the A and B bands of O_2, it is relevant to consider our results in light of previous O_2 A-band line investigations. These include those of Ritter and Wilkerson [40], Schermaul and Learner [66], and Havey *et al.* [67]. All groups reported similar m-dependent deviations between experimental line intensities and the theoretical line lists. For measurements in the P branch, Schermaul and Learner reported a slope of -0.05% per m by comparison of their intensities with those based on the Hönl-London factors of Watson [64]. Using the HITRAN line list as a reference, Havey *et al.* measured O_2 A-band P-branch intensities with FS-CRDS and found the slope to be of the opposite sign and equal to 0.032% per m, and they recalculated the slope of Schermaul and Learner's data to be 0.04% per m. We note that all of these previous slope values were at least a factor of 3 smaller in magnitude than our measured value for the O_2 B band. Schermaul and Learner [66] assigned the m-dependent deviations between measured and theoretical intensities to the Herman-Wallis (HW) effect [68], which is a vibration-rotation interaction influencing the line intensity. For rotating molecules with sufficiently small moments of inertia, the HW effect occurs when the vibrating system does not behave as a rigid rotor, and consequently vibration-rotation interactions become important. This mechanism alters line intensities in absorption [69] and Raman spectra [70]. The present results are consistent with this interpretation, given that the magnitude of our measured slope for the O_2 B band is relatively high in comparison to those reported for the O_2 A band, with the two bands differing only by upper-state vibrational quantum number v'.

V. CONCLUSIONS

We have demonstrated the applicability of our FS-CRDS spectrometer to precise and accurate line-shape and line-intensity measurements of weak O_2 B-band transitions. The line-narrowing effect, which can be equally well modeled as Dicke narrowing or the speed dependence of collisional broadening, turned out to be very important with regard to the line-shape formation of the O_2 transitions investigated here. Use of the Voigt profile with fixed Doppler width in the line-shape analysis causes underestimation of the collisional broadening coefficient by almost a factor of 2 in the extreme case. Moreover, fitting the VP to our measured spectra also causes an incorrect dependence of collisional broadening on rotational energy of the molecule. The strong dependence of fitted collisional parameters on the choice of line profile at low pressures indicates the importance of careful line-shape analysis. This is particularly important for applications based on the precise experimental determination of Doppler line widths such as recent spectroscopic measurements of Boltzmann constant [71–73], for which the collisional narrowing and the speed-dependent effects should not be negligible.

The multispectrum fit procedure applied here significantly reduced the problem of correlation of fitted line-shape parameters at low pressures, thus reducing the uncertainties of our fitted line-shape coefficients. The self-broadening, shifting, and narrowing coefficients which we determined were not reported before. We measured line intensities with subpercent-level uncertainty, which is much better than available data. Our intensities range from 3% to 7.5% greater than values in the HITRAN spectroscopic database. These differences increased quickly with total angular momentum quantum number and illustrate shortcomings of current models that describe the rotational dependence of line intensities for $(b\,^1\Sigma_g^+ \leftarrow X\,^3\Sigma_g^-)$ transitions of O_2.

ACKNOWLEDGMENTS

The authors would like to thank Alan S. Pine for carefully reading the manuscript and offering helpful suggestions. The research is part of the program of the National Laboratory FAMO in Toruń, Poland, and is supported by the Polish MNISW Project Nos. N N202 1255 35 and N N202 1489 33 and by Grant No. JMR UMK 503-F.

[1] J. S. Daniel, S. Solomon, H. L. Miller, A. O. Langford, R. W. Portmann, and C. S. Eubank, J. Geophys. Res. **108**, 4515 (2003).
[2] D. M. O'Brien, S. A. English, and G. Da Costa, J. Atmos. Oceanic Technol. **14**, 105 (1997).
[3] R. Lindstrot, R. Preusker, and J. Fischer, J. Atmos. Oceanic Technol. **26**, 1367 (2009).
[4] C. R. Nowlan, C. T. McElroy, and J. R. Drummond, J. Quant. Spectrosc. Radiat. Transfer **108**, 371 (2007).
[5] R. A. Washenfelder, G. C. Toon, J. F. Blavier, Z. Yang, N. T. Allen, P. O. Wennberg, S. A. Vay, D. M. Matross, and B. C. Daube, J. Geophys. Res. **111**, D22305 (2006).
[6] D. Crisp *et al.*, in *Trace Constituents in the Troposphere and Lower Stratosphere* (Pergamon-Elsevier Science, Kidlington, 2004), Vol. 34, p. 700.
[7] C. E. Miller, L. R. Brown, R. A. Toth, D. C. Benner, and V. M. Devi, C. R. Phys. **6**, 876 (2005).
[8] C. E. Miller *et al.*, J. Geophys. Res. **112**, D10314 (2007).
[9] H. Babcock and L. Herzberg, Astrophys. J. **108**, 167 (1948).
[10] L. P. Giver, R. W. Boese, and J. H. Miller, J. Quant. Spectrosc. Radiat. Transfer **14**, 793 (1974).
[11] A. O'Keefe, Chem. Phys. Lett. **293**, 331 (1998).
[12] J. J. Scherer, J. B. Paul, H. Jiao, and A. O'Keefe, Appl. Opt. **40**, 6725 (2001).
[13] S. Xu, D. Dai, J. Xie, G. Sha, and C. Zhang, Chem. Phys. Lett. **303**, 171 (1999).
[14] V. Motto-Ros, J. Morville, and P. Rairoux, Appl. Phys. B **87**, 531 (2007).
[15] S.-L. Cheah, Y.-P. Lee, and J. F. Ogilvie, J. Quant. Spectrosc. Radiat. Transfer **64**, 467 (2000).
[16] J. E. Barnes and P. B. Hays, J. Mol. Spectrosc. **216**, 98 (2002).
[17] J. T. Hodges, H. P. Layer, W. W. Miller, and G. E. Scace, Rev. Sci. Instrum. **75**, 849 (2004).
[18] J. T. Hodges and R. Ciuryło, Rev. Sci. Instrum. **76**, 023112 (2005).
[19] D. Lisak, J. T. Hodges, and R. Ciuryło, Phys. Rev. A **73**, 012507 (2006).
[20] J. T. Hodges and D. Lisak, Appl. Phys. B **85**, 375 (2006).
[21] D. Lisak, D. K. Havey, and J. T. Hodges, Phys. Rev. A **79**, 052507 (2009).
[22] J.-M. Hartmann, C. Boulet, and D. Robert, *Collisional Effects on Molecular Spectra: Laboratory Experiments and Model, Consequences for Applications* (Elsevier, Amsterdam, 2008).
[23] P. Duggan, P. M. Sinclair, R. Berman, A. D. May, and J. R. Drummond, J. Mol. Spectrosc. **186**, 90 (1997).
[24] L. S. Rothman *et al.*, J. Quant. Spectrosc. Radiat. Transfer **110**, 533 (2009).
[25] P. R. Berman, J. Quant. Spectrosc. Radiat. Transfer **12**, 1331 (1972).
[26] R. H. Dicke, Phys. Rev. **89**, 472 (1953).
[27] R. Blackmore, S. Green, and L. Monchik, J. Chem. Phys. **91**, 3846 (1989).
[28] L. Demeio, S. Green, and L. Monchick, J. Chem. Phys. **102**, 9160 (1995).
[29] S. G. Rautian and I. I. Sobelman, Usp. Fiz. Nauk **90**, 209 (1966) [Sov. Phys. Usp. **9**, 701 (1967)].
[30] A. S. Pine, J. Chem. Phys. **101**, 3444 (1994).
[31] L. Galatry, Phys. Rev. **122**, 1218 (1961).
[32] M. Nelkin and A. Ghatak, Phys. Rev. **135**, A4 (1964).
[33] B. Lance and D. Robert, J. Chem. Phys. **111**, 789 (1999).
[34] R. Ciuryło, A. S. Pine, and J. Szudy, J. Quant. Spectrosc. Radiat. Transfer **68**, 257 (2001).
[35] H. Tran and J.-M. Hartmann, J. Chem. Phys. **130**, 094301 (2009).
[36] R. Blackmore, J. Chem. Phys. **87**, 791 (1987).
[37] R. Ciuryło, D. A. Shapiro, J. R. Drummond, and A. D. May, Phys. Rev. A **65**, 012502 (2001).
[38] P. Joubert, P. N. M. Hoang, L. Bonamy, and D. Robert, Phys. Rev. A **66**, 042508 (2002).
[39] R. M. Herman, Int. J. Spectrosc. **2010**, 306392 (2010).
[40] K. J. Ritter and T. D. Wilkerson, J. Mol. Spectrosc. **121**, 1 (1987).
[41] D. Priem, F. Rohart, J.-M. Colmont, G. Wlodarczak, and J.-P. Bouanich, J. Mol. Struct. **517**, 435 (2000).
[42] R. Wehr, R. Ciuryło, A. Vitcu, F. Thibault, J. R. Drummond, and A. D. May, J. Mol. Spectrosc. **235**, 54 (2006).
[43] F. Rohart, G. Wlodarczak, J.-M. Colmont, G. Cazzoli, L. Dore, and C. Puzzarini, J. Mol. Spectrosc. **251**, 282 (2008).
[44] D. C. Benner, C. P. Rinsland, V. Malathy Devi, M. A. H. Smith, and D. Atkins, J. Quant. Spectrosc. Radiat. Transfer **53**, 705 (1995).
[45] A. S. Pine and T. Gabard, J. Quant. Spectrosc. Radiat. Transfer **66**, 69 (2000).
[46] A. S. Pine and R. Ciuryło, J. Mol. Spectrosc. **208**, 180 (2001).
[47] D. J. Robichaud, J. T. Hodges, L. R. Brown, D. Lisak, P. Masłowski, L. Y. Yeung, M. Okumura, and C. E. Miller, J. Mol. Spectrosc. **248**, 1 (2008).
[48] D. J. Robichaud, J. T. Hodges, P. Masłowski, L. Y. Yeung, M. Okumura, C. E. Miller, and L. R. Brown, J. Mol. Spectrosc. **251**, 27 (2008).
[49] D. A. Long, D. K. Havey, M. Okumura, H. M. Pickett, C. E. Miller, and J. T. Hodges, Phys. Rev. A **80**, 042513 (2009).
[50] B. Lance, G. Blanquet, J. Walrand, and J. P. Bouanich, J. Mol. Spectrosc. **185**, 262 (1997).
[51] J. Ward, J. Cooper, and E. W. Smith, J. Quant. Spectrosc. Radiat. Transfer **14**, 555 (1974).
[52] R. Ciuryło, Phys. Rev. A **58**, 1029 (1998).
[53] G. Nienhuis, J. Quant. Spectrosc. Radiat. Transfer **20**, 275 (1978).
[54] J. O. Hirschfelder, C. F. Curtis, and R. B. Bird, *Molecular Theory of Gases and Liquids* (Wiley, New York, 1954).
[55] M. J. Lindenfeld, J. Chem. Phys. **73**, 5817 (1980).
[56] U. Mingelgrin and R. G. Gordon, J. Chem. Phys. **70**, 3828 (1979).
[57] J. T. Vanderslice, E. A. Mason, and E. R. Lippincott, J. Chem. Phys. **30**, 129 (1959).
[58] P. Duggan, P. M. Sinclair, M. P. LeFlohic, J. W. Forsman, R. Berman, A. D. May, and J. R. Drummond, Phys. Rev. A **48**, 2077 (1993).
[59] P. Duggan, P. M. Sinclair, A. D. May, and J. R. Drummond, Phys. Rev. A **51**, 218 (1995).
[60] R. Ciuryło and J. Szudy, J. Quant. Spectrosc. Radiat. Transfer **57**, 411 (1997).
[61] D. J. Robichaud, J. T. Hodges, D. Lisak, C. E. Miller, and M. Okumura, J. Quant. Spectrosc. Radiat. Transfer **109**, 435 (2008).
[62] J. Zhang, Z. H. Lu, and L. J. Wang, Appl. Opt. **47**, 3143 (2008).
[63] R. R. Gamache, A. Goldman, and L. S. Rothman, J. Quant. Spectrosc. Radiat. Transfer **59**, 495 (1998).

[64] J. K. G. Watson, Can. J. Phys. **46**, 1637 (1968).
[65] G. Herzberg, *Spectra of Diatomic Molecules*, 2nd ed. (D. van Nostrand, New York, 1950).
[66] R. Schermaul and R. C. M. Learner, J. Quant. Spectrosc. Radiat. Transfer **61**, 781 (1999).
[67] D. K. Havey, D. A. Long, M. Okumura, C. E. Miller, and J. T. Hodges, Chem. Phys. Lett. **483**, 49 (2009).
[68] R. Herman and R. F. Wallis, J. Chem. Phys. **23**, 637 (1955).
[69] J. K. G. Watson, J. Mol. Spectrosc. **125**, 428 (1987).
[70] M. Marrocco, Chem. Phys. Lett. **442**, 224 (2007).
[71] C. Daussy, M. Guinet, A. Amy-Klein, K. Djerroud, Y. Hermier, S. Briaudeau, C. J. Bordé, and C. Chardonnet, Phys. Rev. Lett. **98**, 250801 (2007).
[72] G. Casa, A. Castrillo, G. Galzerano, R. Wehr, A. Merlone, D. Di Serafino, P. Laporta, and L. Gianfrani, Phys. Rev. Lett. **100**, 200801 (2008).
[73] K. M. T. Yamada, A. Onae, F.-L. Hong, H. Inaba, and T. Shimizu, C. R. Phys. **10**, 907 (2009).